ARTICLE IN PRESS

ELSEVIER

Materials Science and Engineering A00 (2003) 1–12

MATERIALS SCIENCE & ENGINEERING A

www.elsevier.com/locate/msea

Nitrogen impurity gettering in oxide dispersion ductilized chromium

M.P. Brady [a,*], I.M. Anderson [a], M.L. Weaver [b], H.M. Meyer [a], L.R. Walker [a], M.K. Miller [a], D.J. Larson [a], I.G. Wright [a], V.K. Sikka [a], A. Rar [a,c], G.M. Pharr [a,c], J.R. Keiser [a], C.A. Walls [a]

[a] *Oak Ridge National Laboratory, Oak Ridge, TN 37831-6115, USA*
[b] *University of Alabama, Tuscaloosa, AL, USA*
[c] *University of Tennessee, Knoxville, TN, USA*

Received 13 February 2003; received in revised form 29 March 2003

Abstract

Work by Scruggs in the 1960s demonstrated that tensile ductility could be achieved at room temperature in powder metallurgically-produced Cr alloyed with MgO. During consolidation, much of the MgO converted to the $MgCr_2O_4$ spinel phase, which was hypothesized to getter nitrogen from the Cr, rendering it ductile. We have duplicated this effect, achieving room temperature tensile elongations of 4% for hot-pressed Cr–6MgO–(0–1)Ti (wt.%) and 10% for hot-pressed and extruded Cr–6MgO–0.75Ti. Direct incorporation of nitrogen into the $MgCr_2O_4$ phase was not detected; however, impurities, particularly nitrogen and sulfur, were observed to segregate to and/or precipitate at interfaces between the MgO/$MgCr_2O_4$ phases and the Cr matrix. Exploratory studies of other non-spinel forming oxide dispersions (La_2O_3, TiO_2 and Y_2O_3) showed a similar pattern of impurity segregation/precipitation, suggesting that there is nothing unique about spinel dispersions in Cr with regards to impurities. However, none of these other dispersions resulted in similar levels of tensile elongation.
© 2003 Elsevier Science B.V. All rights reserved.

Keywords: Powder processing; ODS; Composites; Mechanical properties; Segregation; Embrittlement; Cr

1. Introduction

Impurities are a major contributor to the ambient-temperature brittleness of Cr [1]. Transgranular cleavage fracture in Cr has been linked to slip-induced crack initiation at grain boundaries and/or grain boundary impurity precipitates [2,3]. Interstitial impurities have also been associated with reduced mobility of screw dislocations in body-centered cubic (BCC) metals such as Cr, with an accompanying decrease in ductility [4]. Nitrogen is particularly deleterious due to its high solubility in Cr at elevated temperatures, rapidly decreasing solubility with decreasing temperature, and its tendency to form fine, acicular precipitates, often at grain boundaries [1].

The development of Cr as a structural material was aggressively pursued from the late 1950s through the early 1970s [1]. One of the most interesting findings from this era was pioneering work by Scruggs et al. [5,6], who discovered that room temperature tensile ductility could be achieved in commercial-grade Cr with high levels of impurities by the addition of MgO. Blended, sintered, and extruded powders of Cr, MgO, and Ti in the range of Cr–(2–6)MgO–0.5Ti weight percent (wt.%) were reported to exhibit room temperature tensile elongations of up to 20%. Scruggs [5,6] hypothesized that this ductility resulted from the gettering of N and other impurities from the Cr matrix into a $MgCr_2O_4$ spinel phase, which forms from the reaction of MgO and Cr_2O_3 during powder consolidation since commercial purity Cr powder typically contains greater than 0.5 wt.% oxygen. (The 0.5 wt.% Ti was added to the alloys for general gettering purposes.)

The Scruggs Cr–6MgO–0.5Ti alloy was successfully used for components such as a gas turbine flame holder and as a thermowell in an ethylene cracking furnace

* Corresponding author. Tel.: +1-865-574-5153; fax: +1-865-241-0215.
E-mail address: bradymp@ornl.gov (M.P. Brady).

0921-5093/03/$ - see front matter © 2003 Elsevier Science B.V. All rights reserved.
doi:10.1016/S0921-5093(03)00324-1

UNCORRECTED PROOF

after a carburization surface treatment [7]. However, efforts in the 1960s to create environmental-embrittlement-resistant, high-strength Cr and Cr–MgO alloys for demanding high-temperature applications such as gas turbine blades, with a brittle to ductile transition temperature (BDTT) below room temperature, were unsuccessful [1]. Interest in Cr as a high-temperature structural alloy waned in the 1970s, and the work by Scruggs et al. [5–7] has been largely forgotten.

There has been a resurgence of interest in Cr as a structural material [4,8–13], driven by its resistance to high-temperature corrosion, which makes it of great potential utility for the chemical and process industries, and its relatively low coefficient of thermal expansion (CTE), which is attracting attention for application as a metallic interconnector in solid oxide fuel cells [14]. Inadequate room temperature mechanical behavior is still a major limitation. The goal of the present work was to revisit the work of Scruggs, to attempt to replicate the MgO ductilization effect, and to investigate the proposed mechanism of N gettering to provide a basis to guide alloy development efforts devoted to a new generation of oxide dispersion ductilized Cr alloys.

2. Experimental

An ingot of original Cr–6MgO–0.5Ti (wt.%) alloy manufactured in the 1960s was obtained from Dr. Scruggs for study. Details of the processing conditions for this specific ingot were not available; however, these alloys were typically manufactured by sintering blended Cr, MgO, and Ti powders at approximately 1600 °C for 1–2 h and 9:1 extruding at 1200–1300 °C [5,6].

In this study, unalloyed Cr, Cr–0.5Ti, and a series of Cr–6MgO–(0, 0.5, 0.75, 1, 2.2)Ti (wt.%) alloys were made from standard, commercial grade powders (Table 1) of nominal 1–5 μm size range. The MgO powder was calcined and stored in argon to prevent interaction with water vapor. The alloys were typically produced by oblique blending the powders for 24 h using zirconia balls, then hot-pressing under vacuum in a graphite die at ~1600 °C for 2 h at approximately 20 MPa. The cooling rate in the hot-press was relatively slow (under vacuum), taking approximately 30 min to drop below 1000 °C and then on the order of hours to approach room temperature. (The Cr–0.5Ti alloy was made by hot isostatic pressing (HIP) in a Nb can at 1600 °C for 1.5 h at approximately 210 MPa and then cooled to near room temperature in about 1–1.5 h). A hot-pressed Cr–6MgO–0.75Ti alloy was further processed by extruding at 1300 °C with a 9:1 reduction ratio. The original Scruggs alloy and the alloys of the present work were all found to have high levels of N, S, C and O impurities (Table 1).

Table 1
Chemical analysis by inductively coupled plasma and gas fusion (wt.%). The Scruggs alloy data were measured in the present work

Element	Scruggs	Cr–6MgO–0.5Ti	Cr–6MgO–0.75Ti	Cr–6MgO–1Ti	Cr–6MgO	Cr–0.5Ti	Unalloyed Cr	Cr powder	MgO powder
Cr	92.9		93.13	92.05	94.51	98.46	99.07	99.17	–
Mg	3.33		3.43	3.89	3.22	–	–	–	64.88
Ti	0.48		0.71	1.08	–	0.12	–	–	–
O	3.116		2.44	2.7	1.971	0.6027	0.6346	0.59	33.82
N	0.031		0.0406	0.038	0.0326	0.0152	0.0244	0.025	<0.1
C	0.04		0.01	0.06	0.06	<0.01	0.04	0.01	0.11
S	0.019		0.031	0.011	0.015	0.016	0.019	0.02	0.12
Other	0.01Al, 0.02Si, 0.04Fe, 0.01Ca		0.02Si, 0.16Fe, 0.02Ca	0.07Si, 0.1Fe	0.01Si, 0.16Fe, 0.01Ca	0.61Nb, 0.08Si, 0.1Fe	0.01Si, 0.17Fe	0.06W, 0.01Ni, 0.01Al, 0.01Si, 0.09Fe	0.01Na, 0.89Al, 0.04Si, 0.03Fe, 0.1Ca

UNCORRECTED PROOF

Table 2
Room temperature tensile properties (600 grit finish, 3.3×10^{-3} s^{-1} strain rate)

Alloy wt.%, (no. samples)	Yield (MPa)	Fracture (MPa)	% Elongation
Unalloyed Cr (4)	157±6	187±10	1.0±0.3
Cr–0.5Ti (HIP) (3)	181±4	231±14	1.3±0.3
Cr–6MgO (6)	219±12	307±13	4±1
Cr–6MgO (3) (1.5% compressive prestrain)	268±17	317±12	1.1±0.3
Cr–6MgO (1) (3.3×10^{-4} s^{-1} strain rate)	163	323	9.5
Cr–6MgO–1Ti (4)	197±15	334±14	5±1
Cr–6MgO–2.2Ti (3)	318±31	356±17	1±0.4
Cr–6MgO–0.75Ti (5) (hot-pressed/extruded)	227±11	381±16	10±3
Cr–6MgO–0.75Ti (1) (hot-pressed/extruded) (3.3×10^{-4} s^{-1} strain rate)	178	383	18.4
Scruggs Cr–6MgO–0.5Ti (3) (sintered/extruded)	247±7	333±23	8±2
Cr–6La_2O_3 (2)	–	396±12	0
Cr–6La_2O_3 (3) (0.5% compressive prestrain)	–	417±28	0
Cr–6TiO_2 (2)	–	243±16	0
Cr–6TiO_2 (3) (1.5% compressive prestrain)	–	256±10	0
Cr–6Y_2O_3 (2)	–	284±20	0

Samples consolidated by hot-pressing at 1600 °C for 2 h unless otherwise noted.

Hot-pressed alloys of composition Cr–6La_2O_3, Cr–6TiO_2, and Cr–6Y_2O_3 (wt.%) were also made for comparative purposes with the Cr–6MgO alloys, using the same processing conditions. The specific oxides used were selected because, like MgO, they are thermodynamically more stable than Cr_2O_3, but they have different physical properties from MgO and do not form spinel phases with Cr/Cr_2O_3.

Tensile properties of the candidate alloys were evaluated at room temperature in laboratory air using a flat 'dogbone' configuration approximately 0.6–0.7 mm thick with a gage length of 12.7 mm. The samples were prepared to a surface finish of 600 grit (US standard) and tests were typically performed with a crosshead speed of 2.54 mm min^{-1} (initial strain rate of 3.3×10^{-3} s^{-1}). Select tensile samples were also made from rectangular blocks of material compressed 0.5–1.5% parallel to the gage length direction at room temperature to assess the potential importance of mobile dislocation nucleation in the ductilization mechanism.

Microstructures were characterized by optical microscopy, scanning electron microscopy (SEM), in particular using low-voltage energy-dispersive X-ray (LV-EDS) spectrum imaging [15], and electron probe microanalysis (EPMA), using pure element standards for Cr, Mg, and Ti, a BN standard or a Cr_2N standard for N, and an Al_2O_3 standard for O. In an effort to determine the microstructural location of impurities, particularly N, select samples were also characterized by 3D atom probe [16], electron energy loss spectroscopy (EELS) in the transmission electron microscope (TEM), and after in-situ fracture in a scanning Auger nanoprobe (SAN). EELS spectra were acquired under standard conditions ($E = 300$ keV, $\alpha = 3$ mrad, $\beta = 5$ mrad, $0.2 < t/\lambda < 0.4$). To assess the maximum concentration of N in the spinel phase, second difference spectra were formed using standard functions within the Gatan EL/P software. The SAN data was collected at a primary beam voltage of 10 kV and 10 nA, with a primary electron beam diameter of ~20 nm. Compositions from the SAN were determined from a standardless analysis and should be considered semiquantitative. The vacuum was maintained at 5×10^{-10} torr and all data were obtained within 6 h of (in-situ) sample fracture. Under these conditions residual gas absorption of H_2O, CO, and CO_2 on the sample surface is still possible, which may result in artificially high levels of C and O.

3. Results and discussion

3.1. Room temperature tensile properties

The original Scruggs sintered and extruded Cr–6MgO–0.5Ti wt.% alloy exhibited ~8% tensile elongation at room temperature with a 600 grit surface finish and at a strain rate of 3.3×10^{-3} s^{-1} (Table 2), despite high levels of N and other impurities (Table 1). This is a major improvement over the typical room temperature mechanical behavior of Cr, which does not exhibit any appreciable tensile elongation (>1% range) unless the specimens have been electropolished, have a low interstitial impurity (<0.001–0.005 wt.% N), and, usually, have been cold-worked prior to testing [1,2].

Hot-pressed unalloyed Cr and Cr–0.5Ti (HIP) control alloys exhibited tensile elongations of ~1% prior to fracture (Table 2). In contrast, hot-pressed Cr–6MgO alloys exhibited a tensile elongation of ~4%, an improvement over the behavior of the control alloys but still just half of the elongation exhibited by the Scruggs alloy. The addition of Ti to Cr–6MgO at levels of 0.5 and 1 wt.% had little effect on tensile elongation

UNCORRECTED PROOF

(tensile data included for 1 wt.% Ti only), and the addition of 2.2 wt.% Ti significantly increased the yield strength with a reduction in tensile elongation to ~1%. Similar tensile elongations to that exhibited by the original Scruggs alloy were, however, achieved after extruding hot-pressed material with tensile elongation in the range of 10% exhibited by a hot-pressed and extruded Cr–6MgO–0.75Ti alloy (Table 2).

Several additional experiments were conducted to determine if the MgO-dispersed Cr alloys exhibit the classic strain rate sensitivity and notch sensitivity behaviors typical for BCC metals such as Cr [1]. An order of magnitude reduction in tensile strain rate (from 3.3×10^{-3} to 3.3×10^{-4} s^{-1}) resulted in a near doubling of the room temperature tensile elongation (Table 2), with elongation of a hot-pressed Cr–6MgO sample to 9.5% and a hot-pressed and extruded Cr–6MgO–0.75Ti sample to 18.4%. Yield strengths of both alloys were moderately lower, as would be expected with a lower strain rate. This strain rate is comparable to that used in the original Scruggs work, which employed a rate of 1×10^{-4} s^{-1} for the first 0.4% of elongation and then increased to 1×10^{-3} s^{-1}, and matches the 20% range level of tensile elongation originally reported [5,7]. However, a surface finish change from 600 to 180 grit was found to reduce the tensile elongation in the Scruggs alloy (tested at 3.3×10^{-3} s^{-1} strain rate) from 8 to ~2%, indicating that notch sensitivity is reduced at room temperature but not completely eliminated by the addition of MgO. Fracture was predominately cleavage-type in all cases, regardless of the surface finish or the extent of tensile elongation.

For comparative purposes, hot-pressed Cr–6X (wt.%) alloys (X = La_2O_3, TiO_2, or Y_2O_3) were made to survey the effectiveness of alternative oxide dispersions. The La_2O_3 was selected because, like MgO, it exhibits a higher coefficient of thermal expansion (CTE) than that of Cr and would be expected to produce a similar local stress field on consolidation with Cr, the TiO_2 because it exhibits a lower CTE than Cr and is relatively soft like MgO, and Y_2O_3 because of its current use in oxide-dispersed Cr alloys (e.g. Cr–5Fe–1Y_2O_3 [12]). Spinel phases analogous to $MgCr_2O_4$ do not exist in the La–Cr–O, Ti–Cr–O, or Y–Cr–O ternary systems.

All of the hot-pressed Cr–6X alloys exhibited brittle tensile behavior at room temperature, with no measurable plastic tensile elongation (Table 2). The Cr–6Y_2O_3 and, particularly, the Cr–6La_2O_3 were, however, significantly stronger than the Cr–MgO alloys, while the Cr–6TiO_2 alloy exhibited comparable strength to the Cr–MgO alloys. Several tensile samples of hot-pressed Cr–6La_2O_3, Cr–6TiO_2, and Cr–6MgO were also manufactured from material that was compressively prestrained 0.5–1.5% at room temperature (Table 2). No effect of prestrain on the tensile properties of Cr–6La_2O_3 and Cr–6TiO_2 was evident, and they exhibited similar fracture strengths as without prestraining, again without yielding. Prestrain of Cr–6MgO increased the yield strength by ~50 MPa, but reduced tensile elongation to ~ 1%.

3.2. Microstructure

3.2.1. Original Scruggs Cr–6MgO–0.5Ti alloy

The microstructure of the original Scruggs sintered and extruded Cr–6MgO–0.5Ti alloy (Fig. 1) consisted of a nominally pure Cr matrix with aligned bands of MgO and quaternary Mg–Cr–Ti oxide of composition 15Mg–40Cr–10Ti–35O (wt.%) {16Mg–20Cr–58O–6Ti (atomic percent, at.%)}, consistent with a spinel on the $MgCr_2O_4$–Mg_2TiO_4 tie line of approximate composition $2MgCr_2O_4 \cdot Mg_2TiO_4$. No Cr–nitrides or other impurity phases, with the exception of a few isolated examples of Cr carbides, were evident in the microstructure by SEM LV-EDS spectrum imaging. A similar microstructure was also observed for the hot-pressed and extruded Cr–6MgO–0.75 Ti alloy.

Examination of the spinel phase for N was pursued to evaluate the nitrogen gettering mechanism proposed by Scruggs. Scruggs estimated 0.75–1 wt.% N was incorporated into the spinel phase in N-charged Cr–6$MgAl_2O_4$ spinel alloys based on EPMA and mass spectrometer measurements as well as microscopic examination for the appearance of nitride precipitates in the Cr matrix as a function of bulk N content [6]. However, the high concentration of Ti in the spinel phase in the Scruggs Cr–6MgO–0.5Ti alloy examined in the present work complicated the identification of small concentrations of N by EPMA because of the peak overlaps between the N–K and Ti–L lines. The specimens were therefore analyzed by EELS in the TEM.

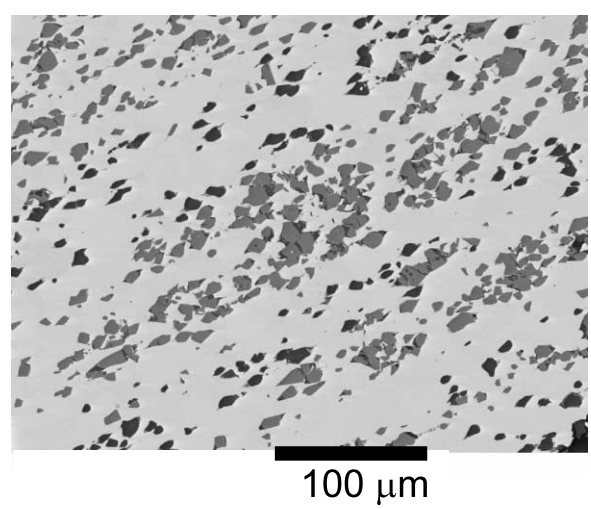

Fig. 1. SEM cross-section micrograph of the Scruggs sintered and extruded Cr–6MgO–0.5Ti wt.% alloy. The light particles are the spinel phase and the dark particles unreacted MgO.

UNCORRECTED PROOF

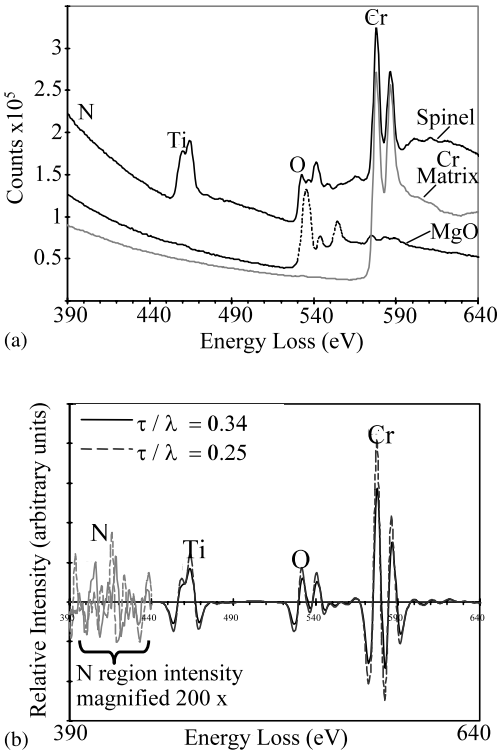

Fig. 2. EELS analysis of the sintered and extruded Scruggs Cr–6MgO–0.5Ti alloy. (a) Raw data; (b) second difference spectra for two different spinel particles with different τ/λ values (τ is sample thickness and λ is inelastic mean free path). Spectral variations in the vicinity of the N edge were uncorrelated between the two second difference spectra, indicating noise.

Representative raw EELS spectra for the Cr matrix, MgO, and spinel phases are shown in Fig. 2a. Characteristic edges for N–K, Ti–L, O–K, and Cr–L are located within this region of the spectrum, as indicated; no characteristic edge for Mg is present. The spectra demonstrate a pronounced enrichment of Ti (consistent with the EPMA analysis), but no visible evidence of N, in the spinel phase. Second-difference spectra, formed to enhance the signal-to-background of the characteristic edges, are shown in Fig. 2b, as acquired from two different spinel particles (a total of six spinel particles were analyzed). Features in the region of the spectrum containing the characteristic N–K edge are magnified by a factor of 200 in Fig. 2b. Spectral oscillations in this N region of the spectrum are consistent with the background noise level.

Assuming N gettering by the spinel phase would result in a concentration enhancement similar to the 20-fold enhancement observed for Ti in the spinel phase in the Scruggs Cr–6MgO–0.5Ti alloy, relative to the bulk composition of the alloy (10 wt.% Ti in the spinel vs. 0.5 wt.% bulk), the concentration of N in the spinel would be expected to be in the range of $\sim$0.6 wt.% (20 times the bulk level of $\sim$0.03 wt.% N; Table 1). This is a factor of $\sim$50 smaller than that of the oxygen in the spinel phase, $\sim$35 wt.% O (i.e. 2% of the anions; refer to O signal shown in Fig. 2b). Such a concentration would result in a N signal several times the noise level in Fig. 2b, which is not observed. Therefore, the EELS measurements showed no evidence of significant gettering of N within the spinel phase.

Atom probe was used to examine the degree to which N was present as a trace element solute in the Cr matrix in the Scruggs alloy. These atom probe measurements did not indicate the presence of N in the Cr matrix, to within the detection limit of the measurement, estimated to be 20 atom parts per million nitrogen (5 wppm) for the sampling of 100,000 atoms. Similar atom probe results were also obtained for a Cr–0.5Ti alloy examined for comparative purposes. The Cr matrix N levels were therefore at least 1–2 orders of magnitude lower than the bulk N levels ($\sim$0.03 wt.%; Table 1), which indicates that the N impurities were not (uniformly at least) concentrated principally in the matrix.

The presence and location of N (and other impurities) in the microstructure of the Scruggs alloy were, however, revealed by in-situ fracture studies in the SAN. Levels of 12–20 at.% N and 10–17 at.% S were detected in pit regions of the fracture surface where oxide particles had been pulled out as shown in the maps in Fig. 3. Similar to the situation with EPMA analysis, N cannot be definitively identified by Auger analysis in microstructural regions where Ti is also locally present due to peak overlaps. The oxide pullout regions marked by arrows in Fig. 3 are locations where no Ti was locally detected-thus the presence of nitrogen at this location could be unambiguously identified. It was not possible to tell whether these sites had held MgO or spinel particles.

Potentially three distinct types of oxide particles, protruding from the fracture surface, were also identified: MgO and two types of Mg–Cr–O base particles, which most likely corresponded to the spinel phase and MgO partially reacted with Cr. The presence of Ca (7–15 at.%), C (5–10 at.%), N (3–7 at.%), Ti ($<$5 at.%), and S ($<$2 at.%) were detected at these Mg–Cr–O particle surfaces, where the concentration of N at these particle surfaces may be overestimated due to the aforementioned peak overlap issues with Ti. No impurities were detected at the MgO particle surfaces; however the absence of impurities here may be an artifact of where the fracture occurred, i.e. the sampled area may have been from within the particle rather than from the original MgO surface | Cr matrix interface. Measurements in the Cr matrix regions of the fracture surface ranged from essentially pure Cr to areas that contained significant levels of C and O impurities, up to 25 at.% each at one site. The areas with high levels of C and O most likely corresponded to grain boundary regions revealed by the fracture, however the primary fracture was transgranular cleavage.

UNCORRECTED PROOF

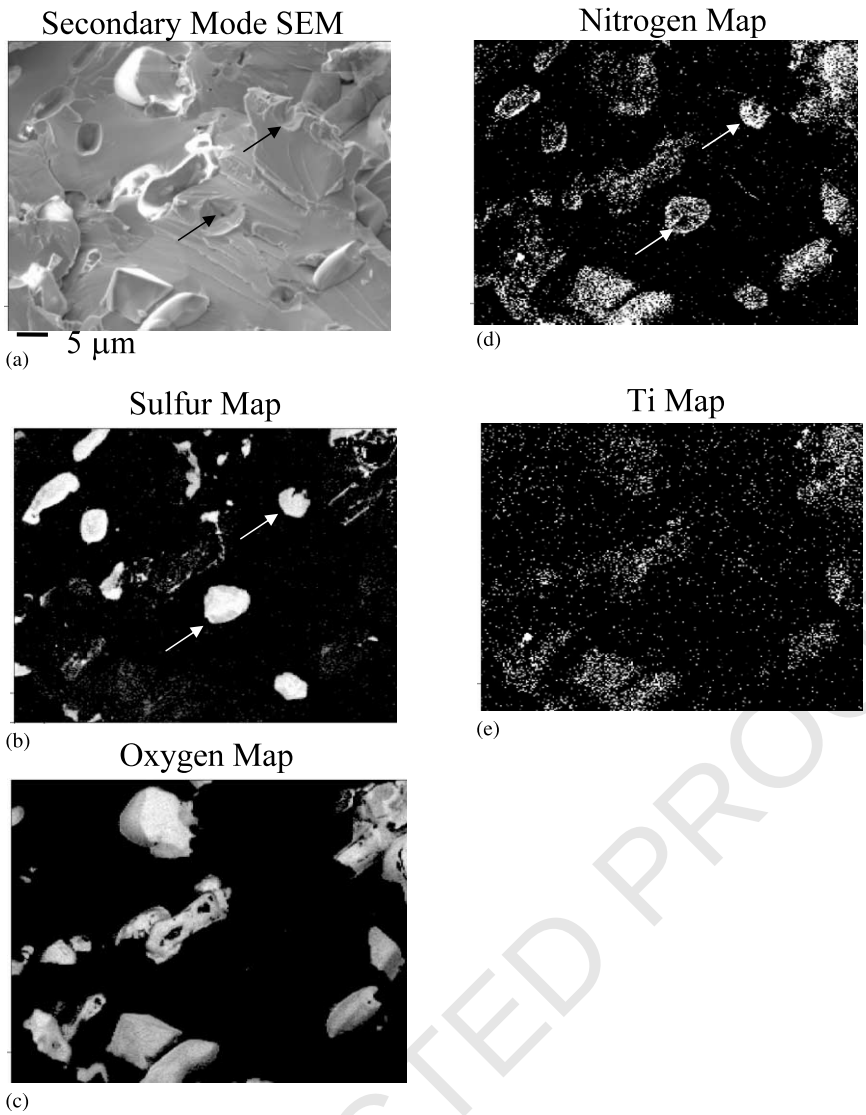

Fig. 3. SAN analysis of in-situ fractured Scruggs Cr–6MgO–0.5Ti alloy. Arrows mark oxide dispersion pull-out regions where N is detected in the absence of Ti. (a) Secondary mode SEM; (b) sulfur map; (c) oxygen map; (d) nitrogen map; (e) titanium map

3.2.2. *Cr–MgO alloys of the present work*

The microstructures of the hot-pressed Cr–MgO alloys of the present work were comparable to that of the Scruggs alloy, although occasional large (~ 50 μm) agglomerations of $MgO/MgCr_2O_4$ particles were observed in hot-pressed alloys (Fig. 4a), but were generally absent in the sintered and extruded Scruggs alloy and the hot-pressed and extruded Cr–6MgO–0.75Ti alloy.

Particles of MgO and a ternary Mg–Cr–O phase were present at the Cr-matrix grain boundaries in hot-pressed Cr–6MgO (Fig. 4a). The composition of the ternary oxide phase was determined by EPMA to be ~12Mg–52Cr–36O wt.% (~ 13Mg–27Cr–60O at.%), consistent with the $MgCr_2O_4$ spinel phase. Nitrogen was not detected in the spinel phase to within the sensitivity limits of the EPMA analysis, estimated to be ~0.05 wt.% in the present work, which is on the order of the bulk level of 0.03 wt.% N in this alloy (Table 1) and an order of magnitude less than the expected level of 0.6 wt.% if spinel phase N gettering had occurred (this alloy was Ti-free and presented no peak overlap issues for N detection). However, the presence of Cr–nitrides in the hot-pressed Cr–6MgO was detected in LV-EDS spectrum imaging (Fig. 4b). The nitrides were relatively coarse and blunt, typically located adjacent to/cupped around the MgO and $MgCr_2O_4$ particles rather than directly on the grain boundaries. Other impurity phases, notably Cr–sulfides and Cr–carbides, were also evident, again relatively coarse and typically located at the $MgO/MgCr_2O_4$ particles.

A similar microstructure was observed for the hot-pressed Cr–6MgO–0.5Ti and Cr–6MgO–1Ti alloys, including impurity phase precipitates primarily at $MgO/MgCr_2O_4$ particles, except that the spinel phase con-

UNCORRECTED PROOF

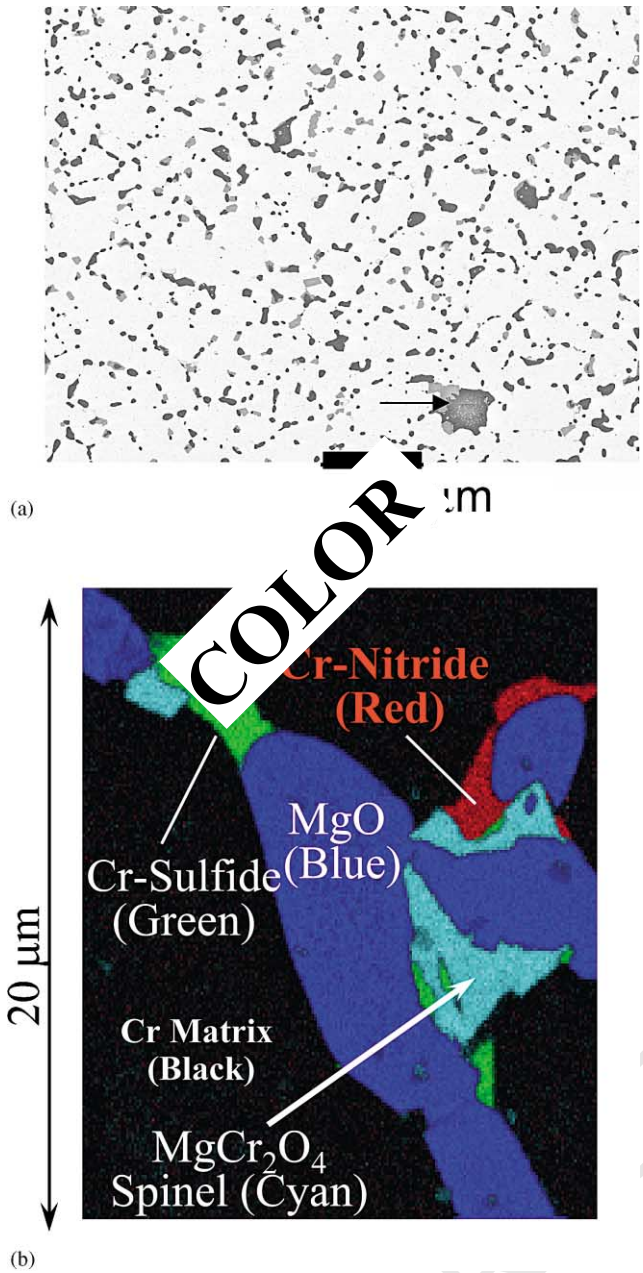

Fig. 4. Microstructure of hot-pressed Cr–6MgO. (a) SEM cross-section micrograph: $MgCr_2O_4$ spinel (light particles), MgO (dark particles). Occasional large particle agglomeration such as that marked by arrows was present. (b) LV-EDS spectrum image phase map of a $MgO/MgCr_2O_4$ particle dispersion area.

tained significant quantities of Ti, as was observed for the Scruggs Cr–6MgO–0.5Ti alloy. In the Cr–6MgO–2.2 wt.% Ti alloy, a ternary Mg–Ti–O phase with less than 1 at.% Cr, rather than $MgCr_2O_4$ base spinel, was present. A range of compositions were measured in the Mg–Ti–O phase regions, varying between 10–30 at.% each of Mg and Ti, suggestive of areas of partial and complete reaction of MgO and Ti/TiO_2 to form Mg_2TiO_4 spinel. Levels of 1–1.5 at.% Ti were also detected in the Cr matrix, which likely contributed to the increased yield strength of this alloy (Table 2) via solid solution hardening.

Analysis of in-situ fractured hot-pressed Cr–6MgO in the SAN revealed similar findings to those observed in the Scruggs alloy. In pit regions in the fracture surface where $MgO/MgCr_2O_4$ particles had been pulled out, N levels of 10–25 at.%, S levels of 5–15 at.%, and, occasionally, C and Ca levels generally less than 10 at.% were detected. Sputtering of the fracture surface at a rate of ~ 0.1 nm min^{-1} (calibrated from SiO_2) decreased the concentration of N and S impurities detected in a pit region from the 10–20 at.% range to less than 2 at.% after 5 min of sputtering. Impurities were also detected at the surfaces of spinel phase particles, typically less than 5–8 at.% each of C and S, with Ca and N also occasionally detected.

3.2.3. Unalloyed Cr and Cr–0.5Ti alloys

The microstructure of the hot-pressed, unalloyed Cr control is shown in Fig. 5a. The grain size was on the order of 0.5 mm, an order of magnitude coarser than the ~ 50 μm grain size present in hot-pressed Cr–6MgO base alloys (e.g. Fig. 4a), and approaching the 0.6–0.7 mm thickness of the tensile samples. The alloy contained a high volume fraction of second phases, primarily Cr_2O_3, distributed throughout the microstructure. LV-EDS spectrum imaging revealed the presence of coarse, acicular Cr–nitrides and Cr–carbides at grain boundaries (Fig. 5b). A similar coarse grain size and acicular grain boundary Cr–nitrides were also observed in Cr–0.5Ti. SAN analysis indicated the presence of N (15–20 at.%), S (13–18 at.%), P (10–20 at.%), and C (<5 at.%) at pit regions in the fracture surface of the hot-pressed unalloyed Cr where pull out of the Cr_2O_3 inclusions occurred (Fig. 6). At the surface of the Cr_2O_3 inclusions, S (8–18 at.%), C (5 at.%), Ca (5–8 at.%), and P (3–5 at.%) were detected.

3.2.4. Other oxide dispersions

The microstructure of the hot-pressed $Cr–6TiO_2$ was qualitatively similar to that observed for hot-pressed Cr–6MgO, while a comparable Cr-matrix grain size but much finer oxide particle size was observed in the $Cr–6La_2O_3$ and $6Y_2O_3$ alloys (Fig. 7). Isolated areas of very large (≥ 100–200 μm) oxide dispersion agglomerations were also present in the $Cr–6TiO_2$ alloy. Approximately 2 at.% Cr was detected in the Y_2O_3 dispersions in the $Cr–6Y_2O_3$ alloy (2Cr–43Y–55O at.%), while the La_2O_3 and TiO_2 reacted extensively with the Cr/Cr_2O_3 during powder consolidation to form ternary phases of average composition 22Cr–20La–58O at.%, consistent with the $LaCrO_3$ phase, and 16Cr–24Ti–60O at.%, respectively. (A number of complex ternary Ti–Cr–O phases exist [17] and an exact determination of the phase formed in the $Cr–6TiO_2$ alloy was not made.) EPMA analysis

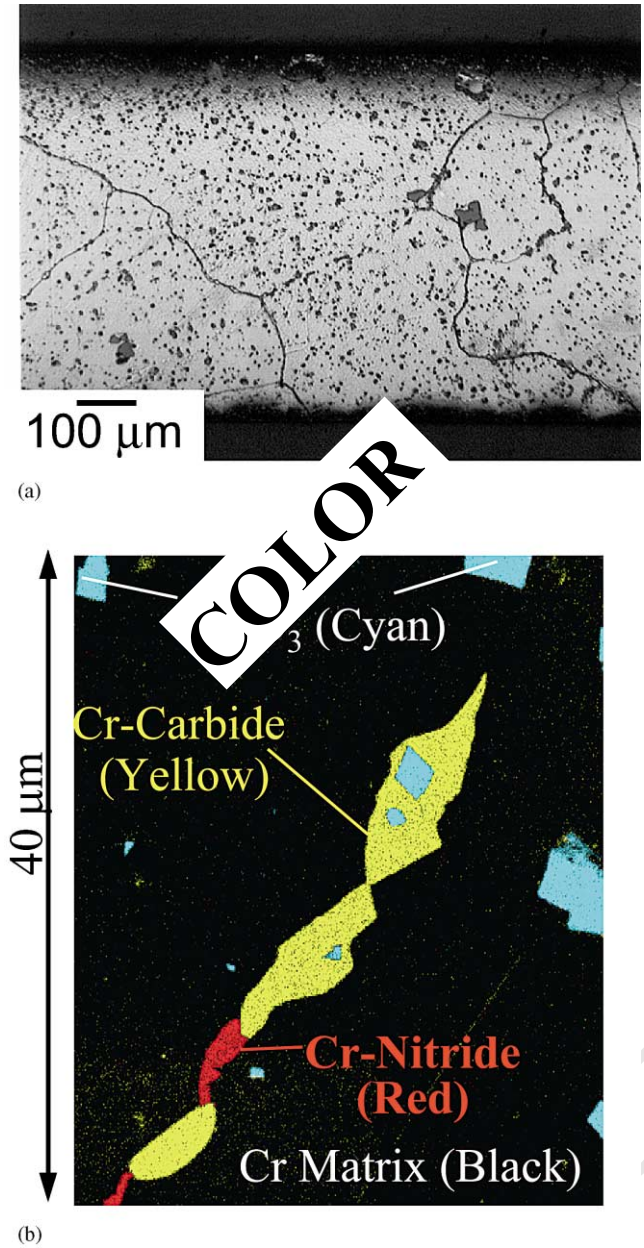

Fig. 5. Microstructure of hot-pressed unalloyed Cr. (a) optical (light microscopy) cross-section (oxalic etch); (b) LV-EDS spectrum image phase map of grain boundary area.

showed no evidence of La, Ti, or Y incorporation into the Cr matrix. Cr–nitride and Cr–sulfide impurity phases, primarily adjacent to oxide dispersions, were observed in Cr–6TiO_2 and Cr–6Y_2O_3 (not examined in Cr–6La_2O_3), similar to those for hot-pressed Cr–6MgO; a typical phase distribution is shown in Fig. 8 for the Cr–6TiO_2 alloy. Further, SAN analysis of in-situ fractured Cr–6Y_2O_3 also showed N and S impurity segregation at oxide pull-out regions in the fracture surface (typically 10–15 at.% each), again similar to that observed in the Cr–6MgO and related alloys.

3.3. Implications

The direct preferential incorporation of N into the $MgCr_2O_4$ spinel phase formed during consolidation of MgO and Cr/Cr_2O_3 powders, as postulated by Scruggs [5,6], was not detected by EELS analysis of the spinel phase in the original Scruggs Cr–6MgO–0.5Ti alloy or by EPMA analysis of the spinel phase in the hot-pressed Cr–6MgO control alloy. Nitrogen and other impurities were, however, observed as segregants at MgO/$MgCr_2O_4$ oxide-dispersion | Cr matrix interfaces in the Scruggs alloy and in hot-pressed Cr–6MgO by SAN analysis. However, the exact chemical form of that segregation remains to be determined. Further, in hot-pressed Cr–6MgO and Cr–6MgO–1Ti, Cr–nitride and Cr–sulfide impurity phases were also observed adjacent to MgO/$MgCr_2O_4$ oxide dispersions in SEM LV-EDS spectrum images. Collectively, the observed pattern of impurity distribution is consistent with the global hypothesis of Scruggs that the addition of MgO to Cr affects the distribution of impurities in Cr, but, in contrast to Scrugg's postulation, it does not appear to occur by direct incorporation into the spinel phase.

These findings are consistent with those of Bakun et al. [18], who linked Cr matrix and grain boundary purification in sintered and extruded Cr–5MgO (0.06 wt.% C and 0.007 wt.% N) to precipitation of impurity inclusions, likely $Cr_{23}C_6$, at MgO | Cr matrix interfaces. They noted 'diffuse' contrast by TEM imaging at grain boundaries in unalloyed recrystallized Cr, associated with segregation of interstitial impurities or very fine interstitial phase precipitates (20–40 nm), as compared to 'banded' contrast in Cr–5MgO, consistent with 'clean' grain boundaries. However, in the present work impurity segregation was also observed at Cr_2O_3 inclusion sites in hot-pressed unalloyed Cr (Fig. 6) and at Y_2O_3 dispersion sites in the hot-pressed Cr–6Y_2O_3 alloy. Additionally, Cr-nitride and Cr–sulfide impurity phase precipitation was observed at complex (non-spinel) Ti–Cr oxide dispersions in Cr–6TiO_2 (Fig. 8) and at Y_2O_3 dispersions in Cr–6Y_2O_3. Therefore, the observed impurity segregation/precipitation does not appear to be unique to, or a special property of spinel phase dispersions in Cr.

This is a key finding because it suggests that efforts to improve the mechanical properties of Cr–MgO and related alloys from an impurity management standpoint do not need to focus on optimization of spinel phase formation during powder consolidation to promote gettering of impurities. Further, it opens up the possibility for the use of other (non spinel) oxide dispersions to provide internal interfaces for impurities to segregate to/precipitate at in Cr. However, although impurity segregation and precipitation were also observed in hot-pressed Cr–6La_2O_3, Cr–6TiO_2 and Cr–6Y_2O_3 alloys, these alloys were brittle under tensile loading at room

UNCORRECTED PROOF

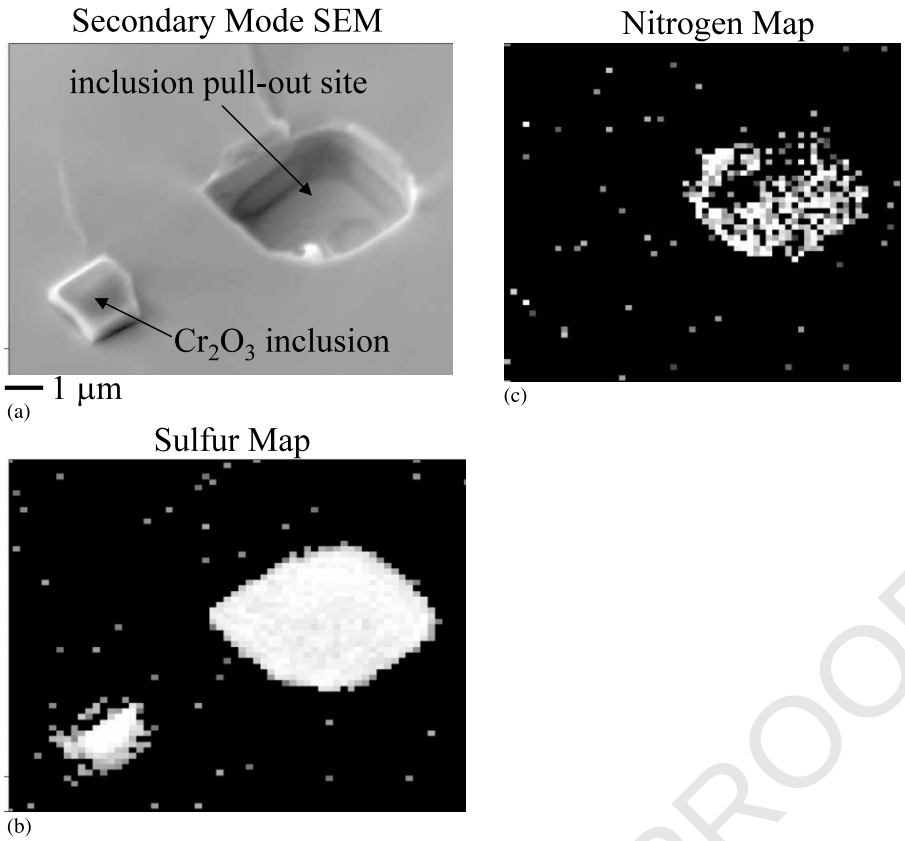

Fig. 6. SAN analysis of in-situ fractured hot-pressed unalloyed Cr. (a) Secondary mode SEM; (b) sulfur map; (c) nitrogen map.

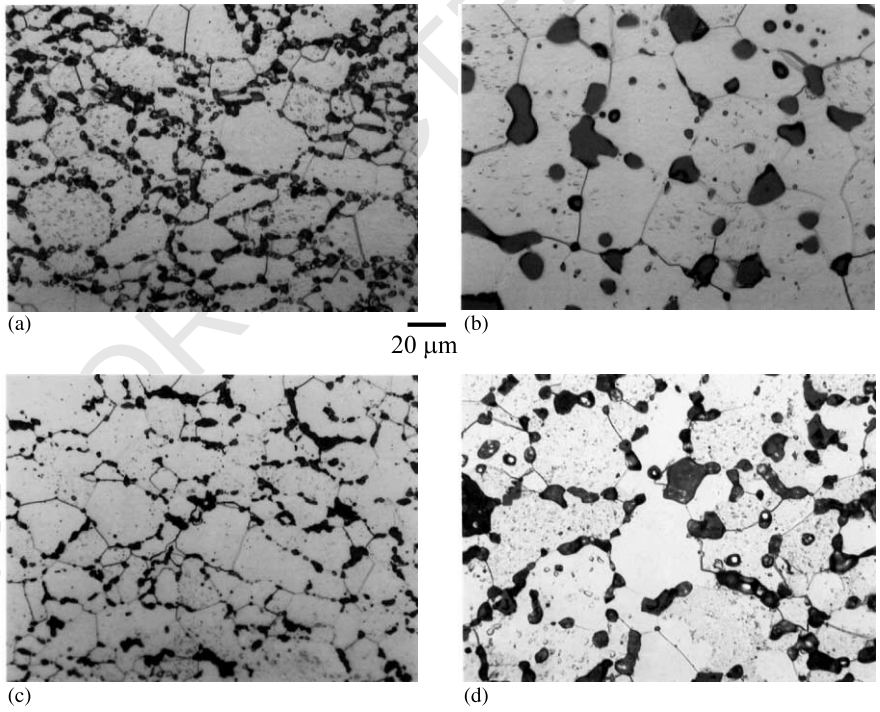

Fig. 7. Optical (light microscopy) cross-section of hot-pressed (a) Cr–6La_2O_3, (b) Cr–6TiO_2, (c) Cr–6Y_2O_3 and (d) Cr–6MgO (oxalic etch). Note that the intragranular features are an etching artifact.

UNCORRECTED PROOF

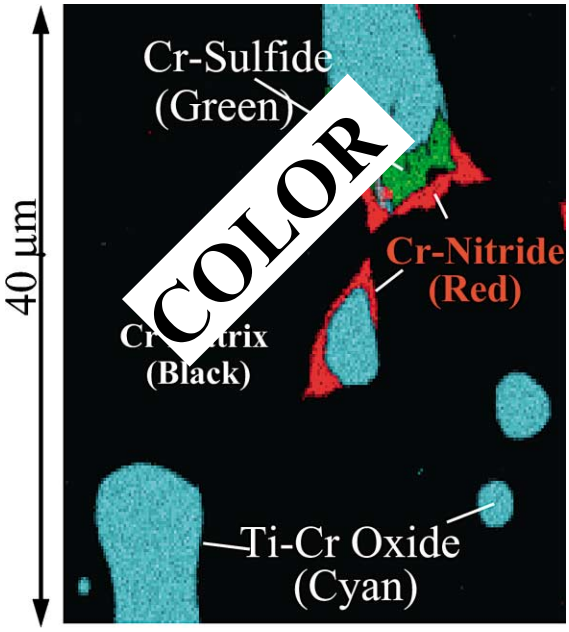

Fig. 8. LV-EDS spectrum image phase map of oxide dispersion region in hot-pressed Cr–6TiO_2.

temperature. Clearly, factors other than impurities must play a major role in determining whether an oxide dispersion is successful in ductilizing Cr at room temperature.

The introduction of fine dispersions has been postulated to improve ductility in bcc metals such as Cr by acting as a mobile dislocation source, decreasing the effective slip plane length, or reducing dislocation pile ups at grain boundaries [2,19]. Surface oxide softening has been reported in bcc metals as well at low homologous temperatures by generation of non-screw dislocations [20–22]. It is not yet clear if these types of mechanisms play a major role in the ductilization of Cr by MgO additions. Based on the absence of an effect of room temperature compressive prestrain on tensile properties of the Cr–6La_2O_3 and Cr–6TiO_2 alloys, and the detrimental effect of compressive prestrain on tensile elongation of Cr–6MgO (Table 2), other factors may supercede the importance of mobile dislocation initiation for achieving tensile elongation in these alloys. Other dispersions, most notably ThO_2 [2], TaC [23], and TiN [24] have been reported to result in ductility of Cr at room temperature, although it is important to note that these effects were observed with electropolished surfaces and with cold work [2] or in bend, and not tensile, tests [23,24]. Scruggs also demonstrated a beneficial effect with the direct addition of $MgAl_2O_4$ spinel to Cr [5–7]; however, the available data suggest that it was not as effective at ductilizing Cr as MgO and that the BDTT was above room temperature.

The observation of Cr nitride and other impurity phase precipitates in the hot-pressed Cr–6MgO and Cr–6MgO–1Ti alloys was surprising given that these alloys showed ~4% tensile elongation at room temperature (Fig. 4). The coarse, blunt morphology of these phases and their location primarily at MgO/$MgCr_2O_4$ particles rather than directly along grain boundaries is thought to help ameliorate their detrimental effects on mechanical properties. The size and morphology of Cr–nitride precipitates have been reported to influence the BDTT of Cr [1], with coarser precipitates, typically formed during slow cooling, as was the case for the hot-press consolidation in the present work, being less detrimental than finer precipitates. The Cr matrix grain size of the Cr–6MgO base alloys was also significantly finer than the unalloyed Cr and Cr–0.5Ti control alloys, which may also have contributed to the improved ductility of these alloys. However, similar coarse impurity precipitates and fine Cr grain sizes were also observed in the Cr– 6La_2O_3, 6TiO_2, and 6Y_2O_3 alloys, which did not exhibit any tensile elongation at room temperature; therefore, these are likely secondary rather than primary factors in determining whether a dispersion is effective in ductilizing Cr.

The presence of any oxide (or other ceramic) dispersion can embrittle Cr at room temperature by acting as local notches, crack initiation sites, or increasing the yield strength relative to the cleavage strength [2], such that the BDTT is raised to above room temperature. These effects can supercede/negate any beneficial effects the dispersions may also have, such as acting as a sink for impurities in the microstructure, and are speculated to be a key factor in the ductilization mechanism. For example, all of the oxide dispersions examined in the present work increased yield strength relative hot-pressed, unalloyed Cr (Table 2), however the increase was much less for MgO additions than for Y_2O_3 and, especially, La_2O_3 additions (e.g. yield strength of 219 MPa for hot-pressed Cr–6MgO vs. fracture strength of 396 MPa, without yielding, for Cr–6La_2O_3, Table 2). The mechanical properties of the dispersion, the nature of the dispersion | metal matrix interface, and the size/distribution/location of the dispersions all play a major role in the resultant mechanical properties of the alloy composite [25,26]. The processing conditions and compositions employed in the present work were based on the Scruggs Cr–MgO work [5–7] and are unlikely to reflect optimal microstructures for the La_2O_3, TiO_2, or Y_2O_3 additions. Preliminary efforts at optimization have yielded a Cr–2TiO_2 wt.% alloy that exhibited a small amount of tensile elongation at room temperature, $1.4 \pm 1\%$ (hot-pressed 1600 °C for 2 h, yield strength of 210 ± 27 and fracture strength of 266 ± 10 MPa, three samples tested). A detailed understanding of the specific factor(s) that led to the inability of the Cr–6La_2O_3, Cr–6TiO_2 and Cr–6Y_2O_3 alloys to exhibit comparable tensile elongations to the Cr–6MgO alloys at room temperature is the subject of ongoing efforts.

UNCORRECTED PROOF

The hot-pressed and extruded Cr–6MgO–0.75Ti alloy exhibited twice the tensile elongation of the hot-pressed Cr–6MgO–(0–1)Ti alloys (Table 2). The increased elongation is primarily attributed to the physical breakup of occasional, large agglomerations of MgO/$MgCr_2O_4$ particles, which were more prevalent in hot-pressed material (e.g. Fig. 4a), by the extrusion treatment. The tensile axis was also aligned with the extrusion direction, and texture/grain size effects resulting from this may also have also played a role in the increased elongation relative to hot-pressed material. Interestingly, impurity phase precipitates (nitrides, carbides, or sulfides), which were observed in hot-pressed material, were rarely observed in the Scruggs sintered and extruded alloy or the hot-pressed and extruded Cr–6MgO–0.75Ti alloy. The elimination of these precipitates during the extrusion treatment by a greater segregation (gettering) of impurities to oxide dispersion | Cr interfaces could also contribute to the improved ductility of the extruded material. For example, Cr starts to exhibit appreciable nitrogen solubility above 1000 °C and the extrusions were performed in the 1200–1300 °C range. However, the possibility that cracking of the impurity phase precipitates during extrusion made them more difficult to retain during metallographic preparation cannot be ruled out.

4. Summary

(1) The addition of 6 wt.% MgO to commercial-grade Cr (high levels of N, S, O, and C impurities) resulted in ~4% tensile elongation at room temperature in hot-pressed alloys and ~10% elongation in hot-pressed/extruded alloys, with a surface finish of 600 grit and a strain rate of 3.33×10^{-3} s^{-1}. The alloys were notch and strain rate sensitive at room temperature, with decreased tensile elongation with a coarser surface finish and increased tensile elongation with decreased strain rates.

(2) Direct incorporation of N and other impurities into the $MgCr_2O_4$ spinel phase, which forms during consolidation of the Cr and MgO powders and was originally postulated to be the mechanism of impurity management in these alloys, was not detected. However, N, S, C, and other alloy impurities were observed to segregate to, and in some cases precipitate at MgO | $MgCr_2O_4$–Cr matrix interfaces.

(3) The observed impurity segregation/precipitation does not appear to be unique to spinel phase dispersions in Cr, as similar impurity segregation and precipitation were also observed at oxide dispersions in hot-pressed Cr–6X wt.% alloys (X = La_2O_3, TiO_2, or Y_2O_3), as well as at Cr_2O_3 inclusions in unalloyed Cr. However, all of the Cr–6X alloys were brittle in tension at room temperature. Factors beyond impurity management must therefore play a major role in determining whether an oxide dispersion is effective in ductilizing Cr. These factors were speculated to include the degree to which the dispersion/resultant dispersed microstructure may act as notches/crack initiation sites or raise the yield stress of the alloy, superceding any beneficial effects the dispersions may also have, such as acting as a sink for impurities.

Acknowledgements

The authors are indebted for the generosity of Dr. D.M. Scruggs in supplying samples of his alloy for study and for many enlightening discussions. The authors thank P.F. Becher, E.P. George, D. Hoelzer, M. Janney, C.T. Liu, R.J. Lauf, J.H. Schneibel and M. Yoo for many helpful discussions and comments on this manuscript. This research was sponsored by the US Department of Energy, Fossil Energy Advanced Research Materials (ARM) Program and the Office of Industrial Technology (OIT) Forest Products Program. The Oak Ridge National Laboratory (ORNL) SHaRE Collaborative Research Center is also gratefully acknowledged. ORNL is managed by UT-Battelle, LLC for the US Department of Energy under contract DE-AC05-00OR22725.

References

[1] W.D. Klopp, NASA TM X-1867, September 1969.
[2] B.A. Wilcox, N.D. Veigel, A.H. Clauer, Met. Trans. 3 (1972) 273.
[3] Y. Matsumoto, S. Ohta, N. Aoki, M. Morinaga, Mater. Sci. Eng. A285 (2000) 213.
[4] U. Holzwarth, H. Stamm, J. Nucl. Mater. 300 (2002) 161.
[5] D.M. Scruggs, US patent 3,175,279 Mar. 30, 1965.
[6] D.M. Scruggs, L.H. Van Vlack, W.M. Spurgeon, J. Am. Ceram. Soc. 51 (1968) 473.
[7] D.M. Scruggs, Mater. Des. Eng. 12 (1962) 115.
[8] H.P. Martinz, W. Kock, T.J. Sakaki, J. Phys. IV 3 (c9, part 1) (1993) 205.
[9] M. Morinaga, T. Nambu, J. Fukumori, M. Kato, T. Sakai, Y. Matsumoto, Y. Torisaka, M. Horihata, J. Mater. Sci. 30 (1995) 1105.
[10] Y. Matsumoto, J. Fukumori, M. Morinaga, M. Furui, T. Nambu, T. Sakaki, Scripta Mater. 34 (1996) 1685.
[11] V. Provenzano, R. Valiev, D.G. Rickerby, G. Valdre, Nanostruct. Mater. 12 (1999) 1103.
[12] A.O. Bilous, L.V. Artyoukh, T.Y. Velikanova, B.D. Bryskin, Int. J. Refractory Hard Mater. 17 (1999) 259.
[13] C.L. Briant, K.S. Kumar, N. Rosenberg, H. Tomioka, Int. J. Refractory Hard Mater. 18 (2000) 9.
[14] W. Kock, H-P Martinz, H. Greiner, M. Janousek, in: M. Dokiya, O. Yamamoto, H. Tagawa, S.C. Singhal (Eds.), Solid Oxide Fuel Cells, vol. IV, ECS, Pennington, NJ, 1995, p. 841.
[15] I.M. Anderson, Microsc. Microanal. 6 (Suppl. 2) (2000) 1048.
[16] M.K. Miller, Atom Probe Tomography, Kluwer Academic/Plenum Publishers, New York, 2000.
[17] H.D. Werner, Neues Jahrb. Miner. Monatsh 5 (1974) 218.

UNCORRECTED PROOF

[18] O.V. Bakun, O.N. Samgina, G.F. Sarhan, V.K. Sul'zhenko, S.A. Firstov, Soviet Powder Metall. Metal Ceram. 20 (4) (1981) 279.
[19] Z. Jiuxing, L. Lu, Z. Meiling, H. Yancao, Z. Tieyong, Int. J. Refractory Hard Mater. 17 (1999) 405.
[20] V.K. Sethi, R. Gabala, Scripta Mater. 9 (1975) 527.
[21] T. Tottori, J.E. Talia, R. Gibala, Scripta Mater. 14 (1980) 1153.
[22] R.D. Noebe, R. Gabala, Scripta Mater. 20 (1986) 1635.
[23] N.E. Ryan, G.R. Wilms, J. Less Common Metals 6 (1964) 201.
[24] N.E. Ryan, S.T.M. Johnstone, J. Less Common Metals 8 (1965) 159.
[25] T.W. Gustafson, P.C. Panda, G. Song, R. Raj, Acta Mater. 45 (4) (1997) 1633.
[26] B.A. Movchan, Mater. Sci. Eng. 72 (1985) 109.

UNCORRECTED PROOF